Brillouin scattering of zero-valent Au-, Cu-, Ag-intercalated hexagonal boron nitride

Bryan W. Reed [●],[1] Catherine Tran [●],[2] and Kristie J. Koski [●][2,*]

[1]*Integrated Dynamic Electron Solutions, Pleasanton, California 94588, USA*
[2]*Department of Chemistry, University of California, Davis, California 95616, USA*

Brillouin laser light scattering spectra of hexagonal boron nitride were measured in its pure form as well as with zero-valent copper, gold, and silver intercalants including one sample co-intercalated with copper and silver. Up to four of the five independent elastic stiffness constants were determined along with the associated sound velocities for the five distinct materials. Intercalation radically changes the optical color of the boron nitride. Brillouin scattering measurements show almost no change in the c_{33} out-of-plane elastic stiffness and the c_{66} in-plane shear modulus, while the c_{11} in-plane stiffness increases by roughly 100 GPa with copper-silver co-intercalation and decreases by roughly 30 GPa with silver intercalation. The results lie within the broad range of literature values for c_{11}, c_{33}, and c_{44} but differ substantially for c_{66}.

I. INTRODUCTION

Zero-valent intercalation is a chemical technique used to change material properties by placing atomic metals, semiconductors, and semimetals into the van der Waals gaps of layered materials [1–3]. Intercalation of zero-valent metals has shown significant ability to alter the optical properties [2,4], acoustic phonons [5,6], electronic transport [2,4,7], and mechanical properties of materials [5,6]. Although there are few measurements of Brillouin scattering of layered materials [6,8–16], intercalation has been shown to have a significant effect on the Brillouin spectra [5,6,17]. Intercalation of Cu, Sn, and Co in α-MoO$_3$ radically alters the mechanical properties measured with Brillouin scattering and significantly increases the shear moduli [5]. Intercalation of Sn into V$_2$O$_5$ has a smaller effect but shows a stiffening of some elastic moduli while others were unaffected or reduced by the Sn intercalant [6]. Intercalation of copper into Bi$_2$Se$_3$ affects the electron-phonon coupling detected with Brillouin scattering [17].

Hexagonal boron nitride (hBN) is a graphite-like, two-dimensional layered insulator with a wide, indirect band gap of 5–6 eV [18]. Hexagonal boron nitride is an ultrahard material with exceptional lubricating properties; it is also ultraexpensive. Given the expense, hBN has primarily found use in cosmetics heightened by its unique shine and luster along with high-end lubrication properties [19,20]. It offers better chemical stability and electrical conductivity than graphite. Intercalating boron nitride with metals could enhance the lubricating properties, add color, and alter the luster—all of which is important for the current and future consumer application of hexagonal boron nitride.

As an intercalation host, hBN is unique because it is challenging to successfully intercalate [21,22]. Of the experimental studies that have been performed, intercalation of Li

into hBN leads to a substantial reduction in the electrical resistivity from 10^{15} to 10^7 Ω cm [23]. Intercalation of Brønsted acids reveals unique molecular bonding environments between the guest and host [24]. Intercalation of potassium leads to new optical transitions but only small charge transfer from guest to host [25].

Further, Caldwell *et al.* proposed that intercalation of atomic species in hBN could enhance and change the nature of the electronic band gap, potentially from indirect to direct gap, by acting as a tensile pressure [26]. Measuring the acoustic phonons and mechanical properties of intercalated hBN allows us to identify whether indeed intercalation of foreign species in hBN leads to modification of the mechanical behavior.

Many computational studies have been pursued to determine the elastic stiffness coefficients of hBN [27–30], but there are only a few experimental studies. These have used ultrasonic techniques [31], inelastic x-ray scattering [32], and Brillouin scattering [13,33]. Jiménez-Riobóo *et al.* measured Brillouin scattering of hexagonal boron nitride in the backscattering geometry on a (0001) surface and the perpendicular facet determining the c_{11} and c_{33} elastic stiffnesses [33]. Brillouin light scattering was collected from the surface phonons of hexagonal boron nitride films deposited using RF and DC sputtering by Wittkowski *et al.* [13]. These measurements show significant deviation in the elastic stiffnesses as compared to theoretical and other experimental measurements with nearly 20 times lower c_{11} stiffness coefficients.

Here, we report Brillouin scattering measurements of commercial hexagonal boron nitride and Ag-, Au-, Cu-, and dual Cu/Ag-intercalated hBN in several scattering geometries. We determine up to four of the five independent elastic stiffness constants (i.e., all but c_{13}, which is challenging to measure in layered materials). Good agreement is shown with experimental and computational literature measurements of unintercalated hBN [33] with the exception of c_{12} where we find values of c_{12} larger than previously reported (or,

---

*koski@ucdavis.edu

equivalently, we find values of c_{66} significantly smaller than previously reported). Intercalation shows substantial change in the optical nature of the crystals with a significant color change associated with intercalation, likely due to the plasmonic nature of the transition metals. Brillouin scattering measurements show almost no change in the c_{33} out-of-plane elastic stiffness and the c_{66} in-plane shear stiffness. For the c_{11} in-plane stiffness, an increase of roughly 100 GPa is found with Cu/Ag co-intercalation and a decrease of roughly 30 GPa for Ag intercalation in hBN. The c_{44} stiffness governing interplanar shear also appears to be sensitive to intercalation. These results suggest zero-valent intercalation as a unique route to alter the acoustic phonons and elastic rigidity of hBN.

II. EXPERIMENTAL DETAILS

Hexagonal boron nitride was obtained from the commercial supplier HQGraphene while all other chemicals were from Millipore Sigma-Aldrich. As crystals were large (>1 mm), intercalation was achieved by modifying established methods for nanoscale crystals (<300 nm) [1–3]. Intercalation reactions were altered to keep atomic percentages of metal intercalant low ($\lesssim$5 atm % in almost all cases) to maintain the hexagonal symmetry of the material. Intercalation of all metals was performed using a vacuum manifold under nitrogen.

Intercalation of copper was performed by placing the hBN crystal under high-purity nitrogen in a two-neck round-bottom flask. A mixture of 0.1 g tetrakisacetonitrile copper hexafluorophosphate in 6 ml of anhydrous acetone was injected into the flask. The intercalation reaction was heated at 48 °C for four hours. After four hours, the crystal was removed and placed into a 25 cm quartz tube in a tube furnace under vacuum (<35 mTorr) at 180 °C for 12 minutes. The crystal was removed and placed back into a two-neck round bottom flask, evacuated, and flushed with nitrogen three times. A solution of 0.17 g tetrakisacetonitrile copper hexafluorophosphate in 6 ml of anhydrous acetone was injected into the flask and the reaction was allowed to sit near reflux at 48 °C for 16 hours. The crystal was removed and placed in a 25 cm quartz tube in a tube furnace and evacuated. The Cu-intercalated hBN was annealed for 15 minutes at 180 °C. Copper is difficult to intercalate into hBN requiring this additional step of intercalation. In a second sample, silver was co-intercalated in a copper-intercalated hBN crystal through self-intercalation from a silver substrate.

Gold was intercalated by a placing the hBN crystal in a two-neck round bottom flask connected to a vacuum manifold. The flask was evacuated and flushed with nitrogen three times. The flask was left under a nitrogen environment. A solution of 0.16 g AuCl in 5 ml of anhydrous acetone was injected into the flask. The reaction was allowed to sit near reflux at 48 °C for 16 hours. The crystal was removed, rinsed with acetone, and annealed in a glass crucible under vacuum in a 25 cm quartz tube furnace for 15 minutes at 180 °C.

Silver was intercalated by placing the hBN crystal in a two-neck round-bottom flask in air. A solution of 0.17 g silver nitrate in 5 ml of acetonitrile and a separate solution of 0.1 g of 1,4,8,11-tetramethyl-1,4,8,11-tetraazacyclotetradecane in 2 ml of acetonitrile was added to the flask. The intercalation reaction was allowed to proceed near reflux at 48 °C for 16 hours. The crystal was removed, rinsed with acetone, and annealed in a glass crucible under vacuum in a 25 cm quartz tube furnace for 15 minutes at 100–180 °C. At very high concentrations of Ag intercalant, the hBN crystals can be destroyed in the annealing step.

Densities of the hBN and intercalated hBN were determined using the linear density gradient method [34]. Several solutions of differing volumes of bromoform (density = 2889 kg/m^3) and ethanol (789 kg/m^3) were mixed together and allowed to sit overnight. These solutions had densities of 1839, 2014, 2102, 2189, 2271, and 2539 kg/m^3. A density gradient was created by carefully layering 0.1 ml of select solutions in a 0.5 ml cylindrical sample vial using a syringe and needle and allowing to sit for an hour. The hBN and intercalated hBN samples were dropped in with a needle and allowed to rise. The density was recorded. The density was further determined by taking the two closest density solutions and floating and/or sinking the hBN crystal. Densities determined are as follows: hBN (2014–2189 kg/m^3); Ag-hBN (2189–2271 kg/m^3); Au-hBN (2189–2271 kg/m^3); Cu-hBN (1839–2189 kg/m^3); AgCu-hBN (2189–2271 kg/m^3). Fused silica (density 2202 kg/m^3) was used as an additional calibrant. The density measurement for pure hBN is consistent with the literature value of 2180 kg/m^3 [35]. Therefore we use the literature value for the density of the unintercalated material. The densities of the Ag-hBN, Au-hBN, and AgCu-hBN were found to lie between 2189 and 2271 kg/m^3. If we suppose a uniform statistical distribution between those two bounds, we arrive at a mean and RMS error of 2230 ± 24 kg/m^3. As for the Cu-hBN, the measurements were more difficult as this form of material tended to deintercalate and exfoliate in liquid suspension. However, we were able to bound the density range to lie between 1839 and 2189 kg/m^3. As it is highly unlikely for the Cu intercalation to lower the density of Cu-hBN relative to hBN, we choose to take the literature density of the unintercalated material as a lower bound. Therefore we take the density of our Cu-hBN sample to be 2185 kg/m^3, halfway between the upper and lower bounds. The dual-intercalated AgCu-hBN did not exfoliate in the bromoform-ethanol solutions.

Brillouin scattering measurements were collected with a Sandercock scanning tandem Fabry-Perot interferometer (TFP-1). A Coherent Verdi V6 Nd:YVO$_4$ laser at $\lambda_0 = 532$ nm was the excitation source. A Mitutoyo M Plan Apo SLWD 20× objective with a numerical aperture of 0.28 was used. The smaller numerical aperture was chosen to minimize the solid angle of collection. Mirror spacing of the etalons was 2–4 mm, depending on scattering geometry and measured crystal direction, with a scan rate of 500 giving a spectral window of 35–70 GHz. Acquisition times ranged from around 10–15 minutes for Cu-hBN and to 3–12 hours for all other hBN samples. Entrance pinholes were kept at 450 μm with an exit pinhole of 700 μm providing an overall system finesse from 120 to ∼350. For 90 degree scattering geometries, a Mitutoyo M Plan Apo 10× long working distance objective with a 0.28 numerical aperture was used as the input lens.
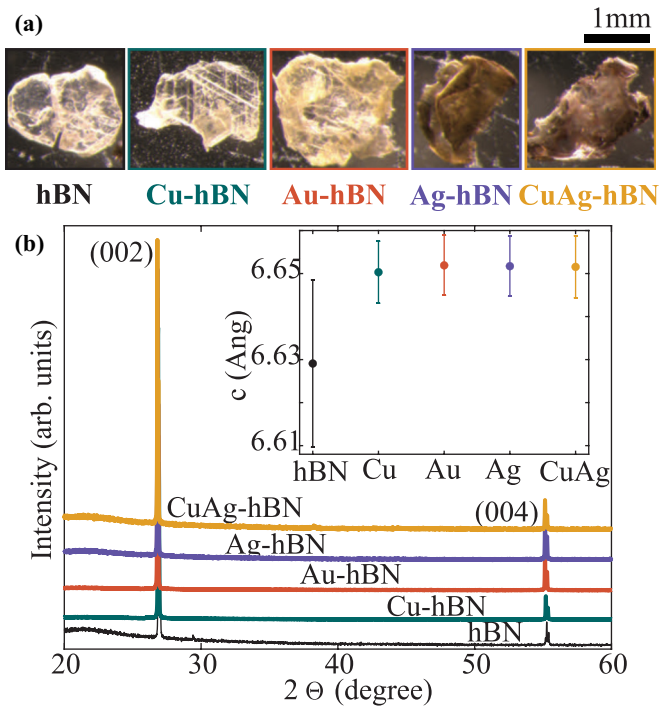
FIG. 1. (a) Optical images of hBN and hBN intercalated with Cu, Au, Ag, and CuAg. (b) XRD of hBN and intercalated hBN showing expansion of the c lattice constant (inset) with intercalation.
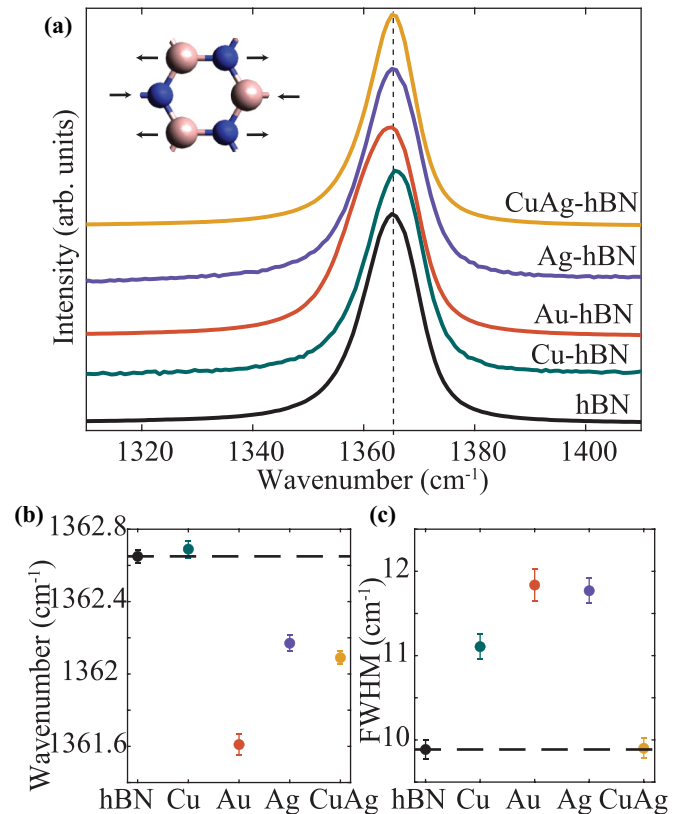

FIG. 2. (a) Raman scattering of hBN and intercalated hBN. Only one mode is measured which corresponds to the (inset) in-plane vibrations. (b) Only a small Raman shift is measured with intercalation. (c) The peak width of Cu-, Au-, and Ag-intercalated hBN increases.

Three scattering geometries were used for Brillouin scattering measurements: 90a, 180, and 90r. In a 90a geometry, the crystal is rotated around the c axis to give a q vector that probes the stiffnesses in the ab plane. The backscattering 180 geometry and 90r geometry are used to measure the refractive index [8] and to measure the elastic stiffnesses in the c direction through the van der Waals layers.

Optical images of hBN [Fig. 1(a)] were collected with a Leica M205C stereoscope. Raman spectra were collected on a home-built microscope that uses a Leica DMi8 inverted microscope, a Princeton Instruments Isoplane SC320, a Princeton Instruments Pixis CCD camera, a Coherent Sapphire SF ultranarrow linewidth laser ($\lambda_0 = 532$ nm), and a Semrock RazorEdge laser filter and dichroic with an edge cutoff of $\sim$38 cm^{-1}. Acquisition times were on the order of 1 second with 1 averaged spectra. All spectra were acquired using an 1800 groove/mm grating.

Scanning electron microscopy (SEM) and energy-dispersive x-ray spectroscopy (EDX) were acquired with a FEI SCIOS dual-beam FIB/SEM using an Oxford EDX detector with 20 keV accelerating voltage and a Thermo Fisher Quattro S Environmental SEM with a Bruker EDX detector operating at 30 keV. X-ray diffraction (XRD) data were acquired using a Bruker D8 Advance Eco with copper K-edge ($\lambda = 1.54$ Å) x rays. X-ray photoelectron spectra (XPS) were acquired using a Kratos Supra Axis with Al anode. Survey spectra were acquired as well as with a sweep of 3 times. High-resolution spectra were acquired with the same sweep time and parameters for all four samples. Low signal is from the thickness and size of the crystals. A neutralizer was used for hBN measurements. Carbon spectra were collected in all high-resolution measurements as a calibrant. The surface was cleaved for XPS measurements. The samples were secured with carbon tape for XPS and SEM measurements.

III. RESULTS AND DISCUSSION

A. Characterization

X-ray diffraction [Fig. 1(b)] shows expansion of the host lattice in the c axis, which is the direction of the van der Waals gap, with intercalation. A noticeable shift to lower values of 2Θ is seen in the (002) peak consistent with expansion of the host. The c lattice constant was calculated from the d spacing of the two observed XRD peaks, (002) and (004), with errors calculated from the standard deviation of the two measurements. As only one lattice direction produced significant peaks, any change in the a-lattice constant could not be determined. The lattice shows expansion in the van der Waals direction associated with a change in the c-lattice constant from 6.63 Å to 6.65 Å. Expansion in the direction of the van der Waals gap is a signature of successful intercalation [3,36]. Typically in layered materials the host initially contracts with intercalation followed by expansion, but in hBN we observe the lattice expanding with even relatively small amounts of intercalant.
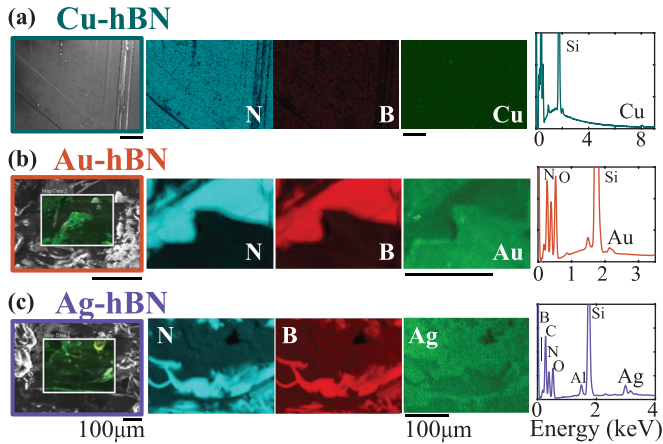
FIG. 3. SEM-EDX map of (a) Cu-intercalated hBN, (b) Au-intercalated hBN, and (c) Ag-intercalated hBN. Scale bar is 100 μm in all images.

Raman scattering spectra [Fig. 2(a)] show the characteristic in-plane phonon [Fig. 2(a); inset] measured at 1362 cm^{-1}. Intercalation very slightly (a decrease of ≲1 wave number) softens this phonon mode for all three intercalants [Fig. 2(b)]. Phonon softening can be caused by expansion of the host or by electron donation of the guest to the hBN [5,6]. The shift in magnitude is small indicating almost no electron-phonon interaction with the host. The peak width increases with intercalation for all but the co-intercalated sample.

Figure 3 shows SEM-EDX maps of the Cu-, Au-, and Ag-intercalated hBN crystals showing distribution of the metals throughout the crystal. EDX spectra are shown next to each map in Fig. 3 with peak identifications showing the presence of each element. The metal peaks are significant in the EDX showing presence of the metal. Such spectra were used to estimate the intercalant concentrations. The nature of the sample, with a very large difference in atomic number between the host and intercalants, made precise quantification very difficult and potentially subject to large systematic errors. As the EDX detector was not windowless, boron was very difficult to detect. Thus, we identify the amount of intercalant per the amount of detected nitrogen. This yielded estimates of 1–4 atm % Cu in hBN, ~5 atm % Au, ~10 atm % Ag, and 1 atm % Cu with 1–3 atm % Ag for the four samples. These values are higher than what would be inferred from the density measurements, assuming small changes in the a lattice constant. Given the likelihood of large systematic errors in the EDX measurements, we choose to use the densities directly determined from the linear density gradient method in analyzing the Brillouin data.

X-ray photoelectron spectroscopy (XPS; Fig. 4) was performed on all samples. The carbon (C 1s) peak was used as a calibrant to shift the binding energies to the same value (280.3 eV) for all samples. As an insulator, hBN suffers from charging effects. The carbon peak was fitted with a Gaussian and an appropriate shift was applied for each spectrum. XPS shows the boron 1s shifts for all intercalants and the nitrogen 1s shifts with Ag intercalation to lower binding energy (higher kinetic energy) with intercalation. The shift to lower binding energy can be explained by the increased electron density
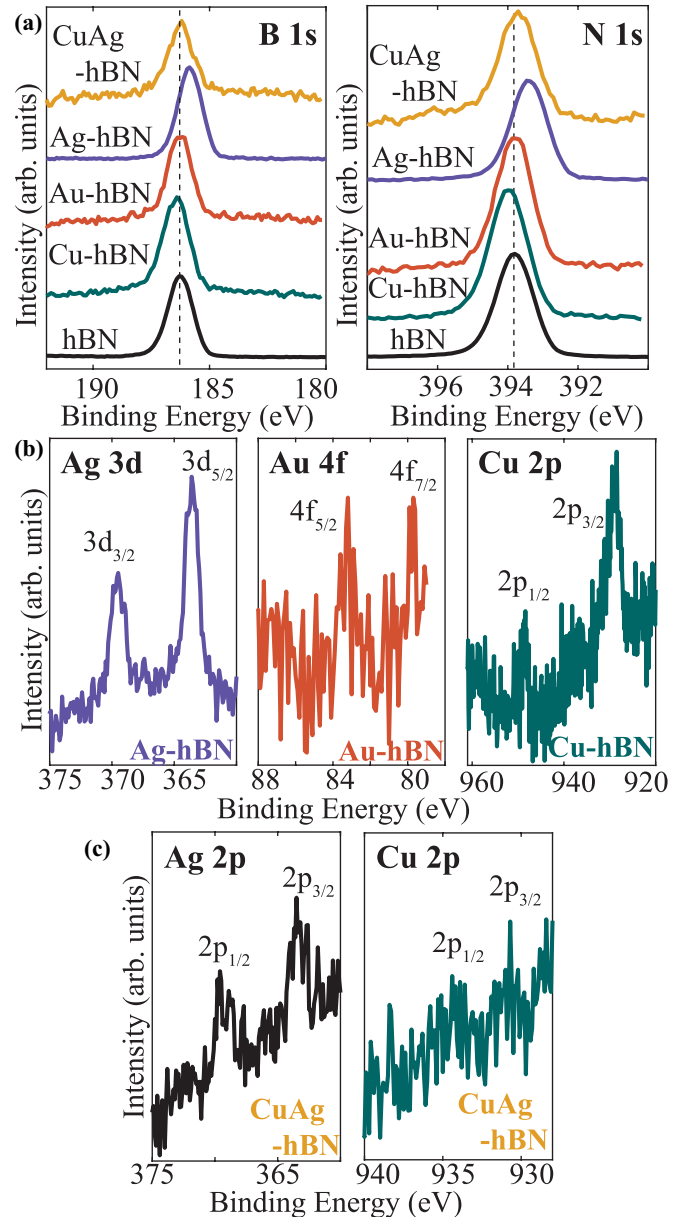

FIG. 4. XPS of (a) the B 1s and N 1s peaks of intercalated hBN, (b) intercalant peaks in Ag-hBN, Au-hBN, Cu-hBN (left to right), and (c) intercalant peaks in CuAg-hBN.

donated by the intercalant leading to better screening of the core electron charges. This has been observed in XPS of many other intercalation compounds [37–39]. The strong shift in the binding energy of the B and N 1s in the Ag-hBN can be attributed to the larger intercalant percentage of Ag. hBN has a surprisingly strong affinity to intercalation of silver. The intercalant percentages from XPS are around ≥1 atm % Cu-hBN, ≲1 atm % Au-hBN, and ≥10 atm % Ag-hBN. The dual intercalated sample yielded values of <1 atm % Cu and ~5 atm % Ag. The XPS confirms that the intercalant percentage is small as found in SEM-EDX but shows a large deviation. Given the thickness of the hBN, and that XPS only probes a few nanometers into the sample, the approximate atomic percent calculated from a survey spectrum can be significantly more
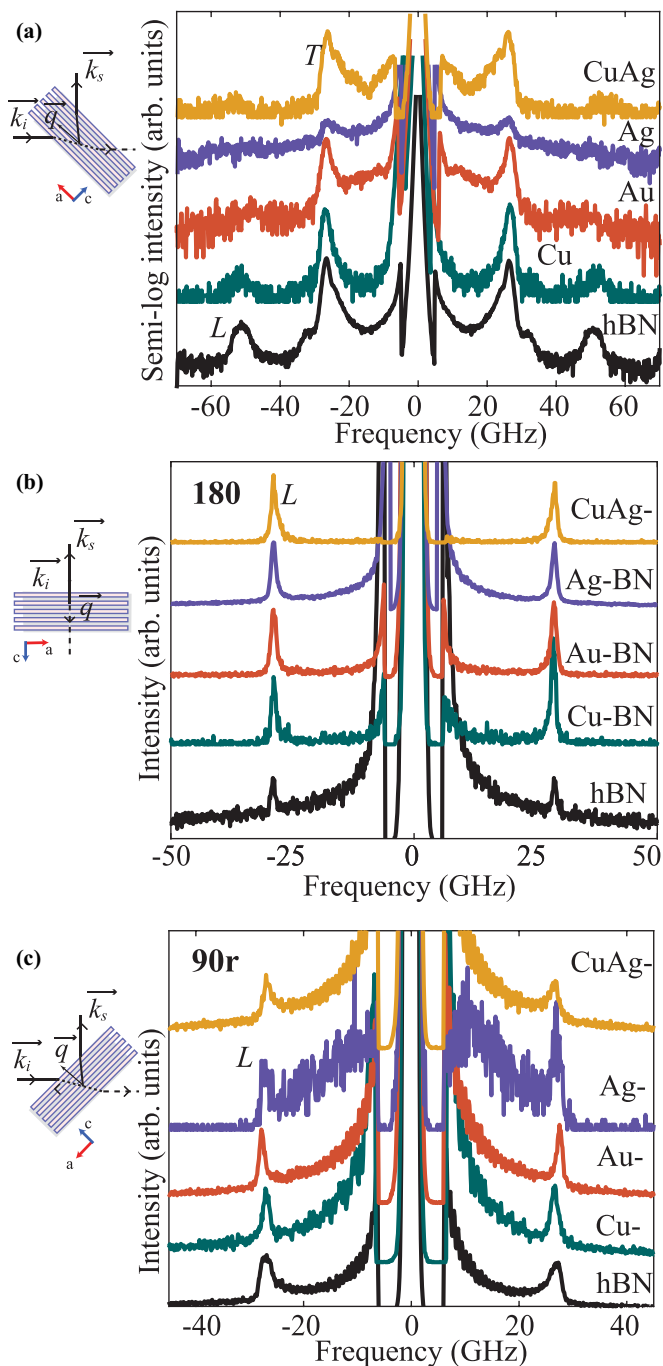
FIG. 5. Brillouin scattering of hBN, Cu-, Au-, Ag-, and CuAg-intercalated hBN in (a) 90a, (b) 180, and (c) 90r scattering geometries.

affected by metals that diffuse in the host with time despite cleaving the sample [40]. Silver and copper are observed in copper-intercalated hBN in both XPS and SEM-EDX.

B. Acoustic phonons: Brillouin scattering

Three scattering geometries were measured with selected data and schematic diagrams shown in Fig. 5 for the geometries: (a) 90a, (b) 180, and (c) 90r. The 90a scattering geometry probes phonons with wave vectors lying in the *ab*
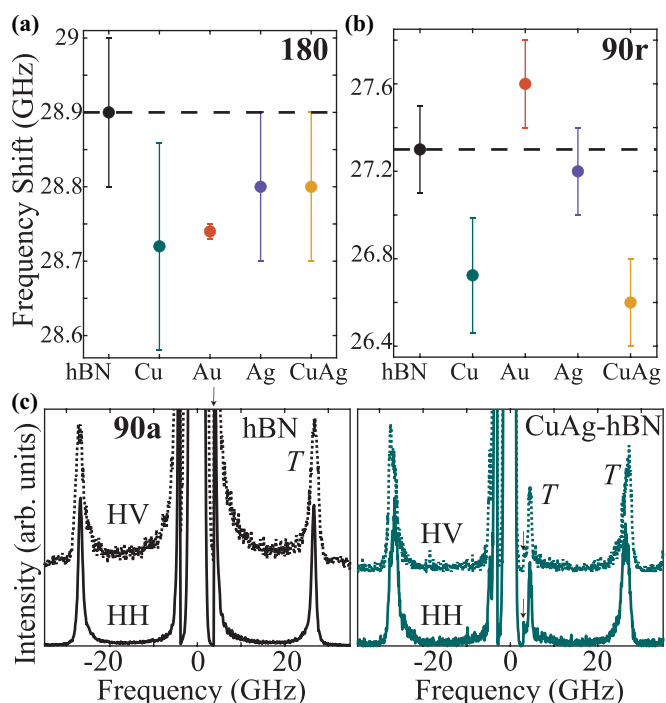

FIG. 6. Brillouin frequency shift of hBN and intercalated hBN in (a) 180 degree geometries and (b) 90r geometries. (c) 90a Brillouin scattering of hBN and CuAg-hBN in HH and HV polarization. Note the doublet at 26 GHz in CuAg-hBN. Shutter edge marked with arrow.

plane. The crystal was rotated around the *c* axis to probe the propagation in multiple directions in the plane. The longitudinal (near 51 GHz) and two transverse (near 26 and 5 GHz) peaks measured in 90a correspond to the c_{11}, c_{66}, and c_{44} (not shown) stiffness coefficients. For a 90a scattering geometry [Eq. (3)], it is not necessary to know the refractive index.

In a 180 backscattering geometry [Fig. 5(b)], only a longitudinal peak, which corresponds to the c_{33} stiffness, is observed due to symmetry rules which prevent the excitation of transverse modes in this case [6,8]. A 90r scattering geometry [Fig. 5(c)] also probes a longitudinal mode corresponding to c_{33}. Assuming linear dispersion, 90r and 180 should measure the same phonon velocity. Quantifying both allows us to verify the measurement while also providing an estimate of the refractive index *n*, as the two geometries have different *n* dependence. While three of the samples produce a refractive index consistent with the literature value of 2.16 [41], we find that Cu and Au intercalation changed the value to 1.93 and 2.53, respectively. This is another indication that the metal is successfully intercalated. Peak positions for 180 [Fig. 6(a)] and 90r [Fig. 6(b)] scattering geometries are presented in Fig. 6 per each intercalant.

Peaks in the 90a scattering geometry were identified through cross and parallel polarizers. In Brillouin scattering, polarizers placed in the back-end optics are used to identify the nature of each peak (Fig. 6). Under cross-polarization of the input light with respect to the scattered light (HV or VH), the longitudinal modes should vanish due to symmetry of the photoelastic tensor, while transverse modes should
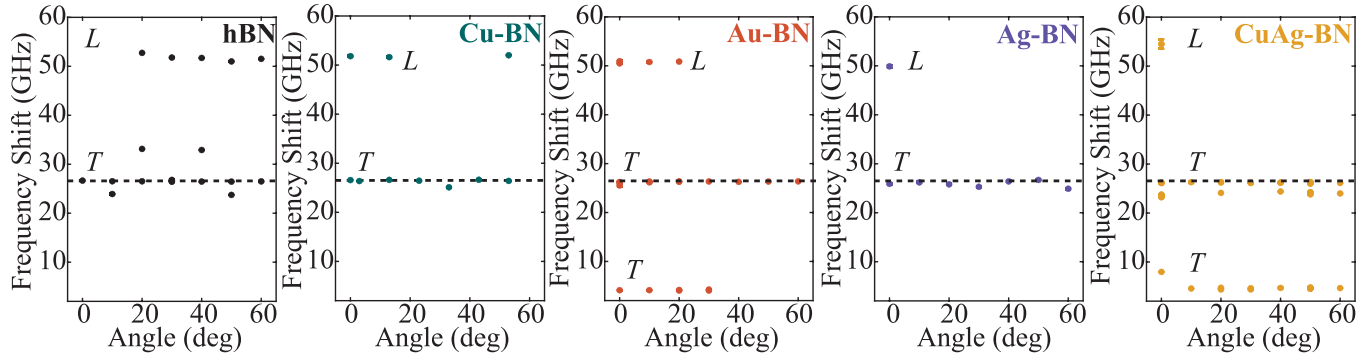
FIG. 7. All peaks seen in Brillouin scattering of pure and intercalated hBN in a 90a geometry as a function of azimuthal angle modulo 60 degrees.

vanish when using parallel polarizers (HH or VV) [6,8]. In 90a, the most intense peak is near 26 GHz. The peak at ∼50 GHz which corresponds to the longitudinal acoustic mode vanishes under cross polarizers. Figure 6(a) shows hBN and Cu-intercalated hBN under cross (HV) and parallel (HH) polarizers. The acoustic mode at 26 GHz does not vanish in hBN or Cu-hBN nor does the peak at 4–5 GHz vanish in Cu-hBN. This identifies both of these modes as transverse or quasi-transverse acoustic modes. In Fig. 6, the cutoff of the slit is identified on the Stokes side with an arrow. Note the large elastic component in hBN (and in Ag-hBN) saturates the transverse mode near 4 GHz making it difficult to measure and extract a c_{44} stiffness, so we were not able to do this for all samples.

As mentioned above, the crystal was rotated about the c axis in a 90a scattering geometry to map out elastic stiffnesses in the ab plane. Peak positions for the 90a geometry are shown for each rotation angle (modulo 60 degrees to respect the hexagonal symmetry of the material) in Fig. 7. Longitudinal and transverse acoustic modes are identified, along with additional unidentified peaks (notably near 24 GHz) that appear in some but not all of the spectra. Theoretically, the linear elastic behavior near the center of the Brillouin zone (as is probed by Brillouin spectroscopy) should show complete in-plane isotropy in a hexagonal material. This is consistent with our observations, in which we see no systematic variation of sound velocities with azimuthal angle. CuAg- and Au-hBN sometimes show a doublet of the transverse mode at around 26 GHz. Similar acoustic phonon mode splitting is seen in different domains of ferroelectrics where it is attributed to different domains of varying dielectric properties within the measured sample region [42,43]. As intercalant metals tend to island with intercalation, it is possible that similar microscopic domains are created in intercalated hBN. We chose to use the higher (∼26 GHz) peak for analysis instead of the lower (∼24 GHz) peak, as the former showed up strongly in nearly every spectrum while the latter was much more weak and variable. A very small but spurious peak is seen around 33 GHz in hBN but only at two angles. Brillouin spectroscopy can be very sensitive to defects and disorder; spurious peaks not describable by basic Brillouin theory are common in many materials. Although large flat areas are chosen for analysis, our hBN samples have many crystal imperfections.

Hexagonal boron nitride has a stiffness tensor of hexagonal symmetry given by Eq. (1):

$$
c_{ij} = \begin{bmatrix}
c_{11} & c_{12} & c_{13} & 0 & 0 & 0 \\
c_{12} & c_{11} & c_{13} & 0 & 0 & 0 \\
c_{13} & c_{13} & c_{33} & 0 & 0 & 0 \\
0 & 0 & 0 & c_{44} & 0 & 0 \\
0 & 0 & 0 & 0 & c_{44} & 0 \\
0 & 0 & 0 & 0 & 0 & c_{66}
\end{bmatrix}, \tag{1}
$$

where $c_{12} = c_{11} - 2c_{66}$ so there are 5 independent moduli. The diagonal components of this matrix directly govern the longitudinal and transverse sound velocities for phonon propagation in the high-symmetry directions in the crystal. Table I presents sound velocities extracted from our measurements. These include the longitudinal sound velocities in and perpendicular to the ab plane ($V_{L\|}$ governed by c_{11} and $V_{L\perp}$ governed by c_{33}, respectively) and pure-transverse sound velocities corresponding to shear in the ab and ac planes ($V_{T_1\|}$ governed by c_{66} and $V_{T_2\|}$ governed by c_{44}, respectively).

In a Brillouin scattering measurement, sound velocities are given by Eq. (2) where V is the sound velocity, $\Delta\nu$ is the measured Brillouin frequency shift, n is the refractive index, λ_0 is the free-space wavelength of laser light ($\lambda_0 = 532$ nm), and Θ is the scattering angle measured inside the material.

$$
V = \frac{\lambda_0 |\Delta\nu|}{2n \sin\left(\frac{\Theta}{2}\right)}. \tag{2}
$$

For the geometries used in this study, this formula yields

$$
V_{90a} = \frac{|\Delta\nu|\lambda_0}{\sqrt{2}}, \tag{3}
$$

$$
V_{180} = \frac{|\Delta\nu|\lambda_0}{2n}, \tag{4}
$$

$$
V_{90r} = \frac{|\Delta\nu|\lambda_0}{\sqrt{4n^2 - 2}}. \tag{5}
$$

In 90a, there is no dependence of the sound velocity upon the index of refraction due to symmetry of the input and collected scattered light. Because the 180 and 90r geometries both probe the same sound speed (longitudinal modes propagating in the c direction) and are subject to the same refractive index in the case of s polarization, it is possible to extract a refractive index from the ratios of these two measurements by

TABLE I. Sound velocity and refractive index of hBN and transition metal intercalated hBN determined by Brillouin scattering in m/s.

	$n_{90r/180}$	$V_{L\parallel}$	$V_{L\perp}$	$V_{T_1\parallel}$	$V_{T_2\parallel}$
hBN	2.16 ± 0.16	$19\,380 \pm 110$	3555 ± 12	9975 ± 11	
Cu-hBN	1.93 ± 0.16	$19\,440 \pm 56$	3533 ± 17	9994 ± 11	
Au-hBN	2.53 ± 0.16	$19\,047 \pm 38$	3536 ± 3	9896 ± 8	1553 ± 27
Ag-hBN	2.16 ± 0.16	$18\,771 \pm 120$	3543 ± 12	9800 ± 75	
Ag-Cu-hBN	2.15 ± 0.16	$20\,510 \pm 380$	3543 ± 12	9866 ± 8	1734 ± 8

solving Eq. (6) for n:

$$\frac{\Delta\nu_{180}}{\Delta\nu_{90r}} = \frac{2n}{\sqrt{4n^2 - 2}}. \qquad (6)$$

These values for n are reported in Table I. However, the values are rather imprecise as Eq. (6) is quite insensitive to n and we have relatively little confidence in these values except as rough estimates. In determining $V_{L\perp}$, we instead chose to use literature values for the relevant refractive index $n_\parallel$ for polarization in the ab plane.

A large range of refractive indices has been reported for hBN from immersion methods [44] and reflectivity [41,45–48] ranging in value from 1.6 to 2.3 for polarization perpendicular and parallel to the ab plane. Following reflectivity measurements by Rah *et al.* [41], we elected to use a value of 2.16 for $n_\parallel$ at 532 nm, which is near the middle of the distributions both of literature values and of our rough estimates from Eq. (6). Previous Brillouin scattering studies used reported refractive indices of hBN as $n_\parallel = 2.304$ and $n_\perp = 1.60$ at 532 nm [47].

Elastic stiffnesses, c_{ij}, are calculated from the sound velocities, V, and the density, ρ, by Eq. (7), where c_{ij} is the stiffness tensor element governing each mode. For the intercalated samples, we use the results from the density gradient method, while for hBN we use [35] 2180 kg/m^3:

$$V = \sqrt{\frac{c_{ij}}{\rho}}. \qquad (7)$$

Table II presents all elastic stiffnesses determined in these measurements. For comparison, experimental and theoretical reported stiffnesses are presented in the same table [27–33].

In a hexagonal crystal, c_{12} and c_{66} are linked by the formula $c_{66} = \frac{1}{2}(c_{11} - c_{12})$. In cases where only one of these two values is reported, the other is obtained using this formula.

The reported literature values, both experimental and computational, of the elastic stiffnesses for hBN vary significantly. As such, our measurements agree very well with this large range of previous measurements and calculations, with the exception of c_{66} and therefore c_{12}. The somewhat lower value of c_{11} seen in a previous Brillouin scattering study [33] may perhaps be attributed to the assumed refractive index value, which is relevant for the 180 backscattering geometry that was used. Our measurements of c_{11} use a 90a scattering geometry which is independent of refractive index [Eq. (3)]. There are other outlying reported values we did not include. For example, Brillouin light scattering of Sezawa waves from hexagonal boron nitride films was measured by Wittkowski *et al.* [13] but the results of the elastic stiffnesses are radically different (e.g., $c_{11} = 38$ GPa) from any other experimental measurement.

Most literature values for c_{66} are in the range 300–380 GPa which would predict a transverse acoustic mode near 34 GHz in a 90a scattering geometry. We observe no reliable peak in this frequency range, with only two weak peaks appearing in this vicinity across the entire set of data. Yet we consistently find a strong peak near 26 GHz, which yields the $\sim$210–220 GPa values we report in the table. While it is conceivable that this peak is misidentified, the lack of any reliable peak at the expected position is still puzzling. This discrepancy is as yet unexplained. The closest literature value to our measurement is from an early theoretical calculation from Green *et al.* [27], but c_{66} was not an independent coefficient in this

TABLE II. Elastic stiffnesses c_{ij} of hBN determined by Brillouin scattering in GPa.

	c_{11}	c_{33}[a]	c_{12}	c_{44}	c_{66}
hBN	819 ± 10	27.6 ± 0.2	385 ± 11		216.9 ± 0.5
Cu-hBN	825 ± 5	27.3 ± 0.3	389 ± 5		218.2 ± 0.7
Au-hBN	809 ± 17	27.9 ± 0.6	373 ± 18	5.4 ± 0.2	218 ± 5
Ag-hBN	786 ± 13	28.0 ± 0.6	358 ± 14		214 ± 6
Ag-Cu-hBN	938 ± 40	28.0 ± 0.6	504 ± 42	6.7 ± 0.1	217 ± 8
Ref. [33] (Exp; Brillouin)	788	24.5			
Ref. [31] (Exp; Ultrasonic)	750	18.7	150	<0.01, 1.52, 2.54	300
Ref. [32] (Exp; Inelastic x-ray)	811	27.0	169	7.7	321
Ref. [27] (Theory; LJ+electrostatic)	802.5	31.2	267.5	3.0	267.5
Ref. [28] (Theory; DFT)	951.5	28.2	169.2	2.5	391.2
Ref. [29] (Theory; DFT 298 K)	863.5	19.3	190.2	7.1	336.7
Ref. [29] (Theory; DFT 0 K)	988.9	58.5	236.5	10.4	376
Ref. [30] (Theory; DFT)	881	33.4	193	5.2	344

[a]Assuming a refractive index $n = 2.16$.

work; the unique methodology implicitly assumes $c_{66} = \frac{1}{3} c_{11}$. Calculations using more modern DFT methods uniformly yielded c_{66} values greater than all of the few available experimental measurements. These experimental measurements, including our own, all used very different techniques and may be subject to different systematic errors related, for example, to defects in the material. Ultrasonic measurements, for example, are known to be susceptible to defects and dislocations in a sample [31]. For now, our results suggest that the in-plane shear modulus c_{66} in hBN may be substantially softer than generally recognized, but as yet the evidence is insufficient to draw any conclusions.

Intercalation affected some elastic moduli much more than others, and the effects vary depending on the intercalant. While copper-silver co-intercalation stiffened the in-plane longitudinal stiffness c_{11} by roughly 100 GPa, pure silver softened it by roughly 30 GPa. Intercalation had very little effect on the out-of-plane longitudinal stiffness c_{33}; in fact, within error this modulus essentially did not change at all. This is surprising, as c_{33} governs the compressibility of the van der Waals gap in which the intercalants reside. After correction for the density changes, there was almost no detectable change in the in-plane shear modulus c_{66} as a result of intercalation. Finally, the out-of-plane shear modulus c_{44} only produced reliable peaks that were not overwhelmed by the Rayleigh peak in two of the samples (with copper-silver dual intercalated and gold intercalation), but these two values differ significantly, indicating that intercalation also modifies c_{44}.

IV. CONCLUSIONS

While hBN has been the subject of many investigations, there are still very few experimental measurements of its elastic properties, and even fewer that obtain most of the independent stiffness coefficients in a single unified methodology. While some of our results for pure hBN are as expected from the literature, others are not, and this suggests areas for further study.

As expected for a hexagonal layered material, we found the sound speeds and elastic moduli of hBN to be isotropic in-plane but highly anisotropic when comparing in-plane and out-of-plane deformation. We observed no systematic variation in the longitudinal and transverse sound velocities in Brillouin scattering measurements that probe phonon propagation in the plane of the crystal. In contrast, when we include out-of-plane propagation the longitudinal modulus varies by roughly a factor of 30 depending on the propagation direction. This is again as expected since in-plane deformation involves stiff, highly directional covalent bonding as opposed to the much softer van der Waals and dipole-dipole interactions that couple each plane to its neighbors. Our measurements of c_{11}, c_{33}, and c_{44} fall well within the range of literature values, while our measurements of c_{66} consistently yield values substantially smaller than expected. This discrepancy is unexplained, and it may be worthwhile to investigate it further using a variety of experimental and computational methods.

Intercalation of copper, silver, and gold modified the elastic moduli in unexpected ways. The largest absolute changes were in the in-plane longitudinal stiffness, while we detected essentially no change in the longitudinal stiffness in the plane-normal direction. This suggests that for longitudinal deformation the presence of the intercalant is, unexpectedly, having more effect on the stiffness of the B-N covalent bonds than on the interlayer interactions across the van der Waals gap. In contrast, intercalation had a fairly subtle effect on the in-plane shear modulus, while the two available values for the out-of-plane shear modulus show a difference of over 20% between the CuAg- and Au-intercalated forms. This suggests nearly the opposite conclusion in the case of shear deformation: that the intercalants had relatively little effect on the rigidity of the B-N covalent bond network while substantially modulating the ability to transfer shear stress across the van der Waals gap. That intercalation could have such different effects on longitudinal versus shear deformation modes is, in our view, among the more surprising outcomes of this study.

A variety of mechanisms could be at play in the effect of intercalation on the elastic moduli. Direct charge transfer between the noble metal intercalants and the valence and conduction bands (i.e., the bonding and antibonding orbitals) of the hBN may be involved, as may electron-phonon coupling similar to other metal intercalants in hBN [49]. The presence of polarizable atoms in the gap may affect both the van der Waals and dipole-dipole interplanar interactions. The band gap of hBN is quite large (6.08 eV), and that may contribute to relatively small charge transfer between the host and the intercalant as previously observed in the case of potassium intercalant [25].

Further, it is worth noting that both copper-containing samples required a significantly shorter Brillouin acquisition time ($\sim$10 minutes versus $\sim$6–10 hours) for the same signal quality even at low intercalant concentrations of copper. It is possible that some indirect plasmon enhancement or other scattering-enhancement mechanism occurs with this low concentration of copper metal at this laser wavelength (532 nm) [50].

In terms of applied potential of intercalated hBN, this study shows that metal intercalation can change the crystal color while maintaining the exceptional shear mechanical properties. This offers promising potential for enhancing current consumer applications, especially in cosmetics, of hBN.

[1] K. J. Koski, J. J. Cha, B. W. Reed, C. D. Wessells, D. Kong, and Y. Cui, J. Am. Chem. Soc. **134**, 7584 (2012).

[2] K. J. Koski, C. D. Wessells, B. W. Reed, J. J. Cha, D. Kong, and Y. Cui, J. Am. Chem. Soc. **134**, 13773 (2012).

[3] M. Wang, D. Williams, G. Lahti, S. Teshima, D. D. Aguilar, R. Perry, and K. J. Koski, 2D Mater. **5**, 045005 (2018).

[4] C. Stern, A. Twitto, R. Z. Snitkoff, Y. Fleger, S. Saha, L. Boddapati, A. Jain, M. Wang, K. J. Koski, F. L. Deepak, A. Ramasubramaniam, and D. Naveh, Adv. Mater. **33**, 2008779 (2021).

[5] B. W. Reed, D. R. Williams, B. P. Moser, and K. J. Koski, Nano Lett. **19**, 4406 (2019).

[6] B. W. Reed, V. Huynh, C. Tran, and K. J. Koski, Phys. Rev. B **102**, 054109 (2020).

[7] Y. Gong, H. Yuan, C.-L. Wu, P. Tang, S.-Z. Yang, A. Yang, G. Li, B. Liu, J. van de Groep, M. L. Brongersma, M. F. Chisholm, S.-C. Zhang, W. Zhou, and Y. Cui, Nat. Nanotechnol. **13**, 294 (2018).

[8] B. W. Reed and K. J. Koski, J. Appl. Phys. **131**, 165109 (2022).

[9] L. E. McNeil and M. Grimsditch, Phys. Rev. B **44**, 4174 (1991).

[10] S. Nakashima, H. Katahama, M. Daimon, and A. Mitsuishi, Solid State Commun. **31**, 913 (1979).

[11] J. Sandercock, Some recent applications of Brillouin scattering in solid state physics, in *Festkörperprobleme 15* (Springer, Berlin, 1975), pp. 183-202.

[12] E. Tato, T. Komatsu, and Y. Kaifu, J. Phys. Soc. Jpn. **54**, 3597 (1985).

[13] T. Wittkowski, P. Cortina, J. Jorzick, K. Jung, and B. Hillebrands, Diam. Relat. Mater. **9**, 1957 (2000).

[14] S. Lee and S. Lindsay, Phys. Status Solidi B **157**, K83 (1990).

[15] M. Grimsditch, Surface Brillouin scattering from graphite, Tech. Rep. No. ANL/MSD/PP-77687, Argonne National Lab. (ANL), Argonne, IL, USA, 1992.

[16] A. Trzaskowska and B. Mroz, Sci. Rep. **10**, 11812 (2020).

[17] M. Wiesner, K. Koski, A. Laitinen, J. Manninen, A. A. Zyuzin, and P. Hakonen, Sci. Rep. **12**, 12097 (2022).

[18] G. Cassabois, P. Valvin, and B. Gil, Nat. Photonics **10**, 262 (2016).

[19] L. M. S. Ansaloni and E. M. B. de Sousa, Mater. Sci. Appl. **4**, 22 (2013).

[20] M. M. Fiume, Jr., W. F. Bergfeld, D. V. Belsito, R. A. Hill, C. D. Klaasen, D. C. Liebler, J. G. Marks, Jr., R. C. Shank, T. J. Slaga, P. W. Snyder, and F. A. Andersen, Int. J. Toxicol. **34**, 53S (2015).

[21] S. N. Shirodkar and E. Kaxiras, Phys. Rev. B **93**, 245438 (2016).

[22] B.-Q. Dai and G.-L. Zhang, Mater. Chem. Phys. **78**, 304 (2003).

[23] A. Sumiyoshi, H. Hyodo, and K. Kimura, J. Phys. Chem. Solids **71**, 569 (2010).

[24] N. I. Kovtyukhova, Y. Wang, R. Lv, M. Terrones, V. H. Crespi, and T. E. Mallouk, J. Am. Chem. Soc. **135**, 8372 (2013).

[25] G. Doll, J. Speck, G. Dresselhaus, M. Dresselhaus, K. Nakamura, and S.-I. Tanuma, J. Appl. Phys. **66**, 2554 (1989).

[26] J. D. Caldwell, I. Aharonovich, G. Cassabois, J. H. Edgar, B. Gil, and D. N. Basov, Nat. Rev. Mater. **4**, 552 (2019).

[27] J. Green, T. Bolland, and J. Bolland, J. Chem. Phys. **64**, 656 (1976).

[28] N. Ohba, K. Miwa, N. Nagasako, and A. Fukumoto, Phys. Rev. B **63**, 115207 (2001).

[29] Y. Qi and L. G. Hector Jr., Appl. Phys. Lett. **90**, 081922 (2007).

[30] L. Xiao, W. J. He, and Y. S. Yin, Ad. Mat. Res. **79**, 1337 (2009).

[31] L. Duclaux, B. Nysten, J.-P. Issi, and A. W. Moore, Phys. Rev. B **46**, 3362 (1992).

[32] A. Bosak, J. Serrano, M. Krisch, K. Watanabe, T. Taniguchi, and H. Kanda, Phys. Rev. B **73**, 041402(R) (2006).

[33] R. J. Jiménez-Riobóo, L. Artús, R. Cuscó, T. Taniguchi, G. Cassabois, and B. Gil, Appl. Phys. Lett. **112**, 051905 (2018).

[34] G. Oster and M. Yamamoto, Chem. Rev. **63**, 257 (1963).

[35] *Semiconductors: Group IV Elements and III-V Compounds*, edited by O. Madelung (Springer-Verlag, Berlin, 1991).

[36] A. Powell, Annu. Rep. Prog. Chem. Sect. C: Phys. Chem. **90**, 177 (1993).

[37] S. Södergren, H. Siegbahn, H. Rensmo, H. Lindström, A. Hagfeldt, and S.-E. Lindquist, J. Phys. Chem. B **101**, 3087 (1997).

[38] H. Estrade-Szwarckopf and B. Rousseau, Synth. Met. **23**, 191 (1988).

[39] J. Swiatowska-Mrowiecka, S. de Diesbach, V. Maurice, S. Zanna, L. Klein, E. Briand, I. Vickridge, and P. Marcus, J. Phys. Chem. C **112**, 11050 (2008).

[40] A. L. Gross, L. Falling, M. C. Staab, M. I. Montero, R. R. Ullah, D. M. Nisson, P. Klavins, K. J. Koski, N. J. Curro, V. Taufour, S. Nemsak, and I. Vishik, J. Phys. Mater. **5**, 044005 (2022).

[41] Y. Rah, Y. Jin, S. Kim, and K. Yu, Opt. Lett. **44**, 3797 (2019).

[42] M. Aftabuzzaman and S. Kojima, Jpn. J. Appl. Phys. **55**, 07KB03 (2016).

[43] M. Rahaman, T. Imai, T. Sakamoto, and S. Kojima, Integr. Ferroelectr. **185**, 22 (2017).

[44] T. Ishii and T. Sato, J. Cryst. Growth **61**, 689 (1983).

[45] D. Jin-Xiang, Z. Xiao-Kang, Y. Qian, W. Xu-Yang, C. Guang-Hua, and H. De-Yan, Chin. Phys. B **18**, 4013 (2009).

[46] O. Stenzel, J. Hahn, M. Röder, A. Ehrlich, S. Prause, and F. Richter, Phys. Status Solidi A **158**, 281 (1996).

[47] A. Segura, L. Artús, R. Cuscó, T. Taniguchi, G. Cassabois, and B. Gil, Phys. Rev. Mater. **2**, 024001 (2018).

[48] S.-Y. Lee, T.-Y. Jeong, S. Jung, and K.-J. Yee, Phys. Status Solidi B **256**, 1800417 (2019).

[49] N. H. Shimada, E. Minamitani, and S. Watanabe, Appl. Phys. Express **10**, 093101 (2017).

[50] W. M. Robertson, A. L. Moretti, and R. Bray, Phys. Rev. B **35**, 8919 (1987).